Available online at www.sciencedirect.com
ScienceDirect
Planetary and Space Science 57 (2009) 23–33
Planetary and Space Science
www.elsevier.com/locate/pss

Electric potential jumps in the Io-Jupiter flux tube

S. Hess[a,b,*], P. Zarka[b], F. Mottez[a], V.B. Ryabov[c]

[a]LUTH, Observatoire de Paris, CNRS, Université Paris Diderot, 5 Place Jules Janssen, 92190 Meudon, France
[b]LESIA, Observatoire de Paris, CNRS, UPMC, Université Paris Diderot, 5 Place Jules Janssen, 92190 Meudon, France
[c]Complex Systems Department, Future University Hakodate, 116-2 Kamedanakano-cho, Hakodate-shi, Hokkaido 041-8655, Japan

Received 28 May 2008; received in revised form 17 September 2008; accepted 7 October 2008
Available online 29 October 2008

Abstract

The Io flux tube (IFT), along which Io interacts with the Jovian magnetosphere, is the place of plasma acceleration processes resulting in auroral like emissions, in UV, IR and Radio emissions in the decameter range. At Earth, the study of the acceleration processes is mainly made by in situ measurements. Acceleration processes at Jupiter were first deduced from the observation of a particular kind of decameter radio emissions from the IFT: the short (S-)bursts. These radio bursts present a negative drift in the time–frequency domain, which is related to the motion of the energetic electrons which produce them. The measure of their drift thus permits the kinetic energy of the electrons to be obtained, as well as its variations along the IFT which have been interpreted as electric potential jumps. Using an enhanced S-burst detection and drift measurement method, more than 1 h of quasi-continuous decametric emissions recorded at the Kharkov UTR-2 radiotelescope have been analyzed. We observe the evolution of the electron kinetic energy with the longitude of Io with a resolution of ~10 s, and detect the presence of acceleration structures with characteristics being consistent with electric potential jumps of few hundred volts, and moving along the IFT in the upward direction (toward Io) at the local sound velocity.

Keywords: Jupiter-Io interaction; S-bursts; Radio emissions; Electrons acceleration; Potential drops

1. Introduction

Io's orbit around Jupiter is surrounded by a dense plasma torus (Bagenal, 1994; Moncuquet et al., 2002) which is nearly in corotation with the Jovian magnetic field. Thus Io moves relative to its plasma torus and the frozen-in Jovian magnetic field. This motion generates an intense corotational electric field (Goldreich and Lynden-Bell, 1969; Saur et al., 2004) and a magnetic field perturbation (Delamere et al., 2003) which leads to the propagation of Alfvén waves carrying electric currents along the Io flux tube (IFT) (Neubauer, 1980; Saur, 2004). These Alfvén waves can resonate within the IFT, near the Jovian ionosphere, and the resonant cavity can select a few privileged resonance frequencies (Su et al., 2006). These waves may accelerate the electrons in the IFT. Due to the partial reflection of the electron population by the magnetic mirror effect at low altitude, the electron population acquires distributions unstable relative to the cyclotron-maser instability. This permits to the energetic electrons to generate intense radio emissions (Wu and Lee, 1979; Wu, 1985). The duration and the structure of the emissions depends on the acceleration process. Long duration arcs (Queinnec and Zarka, 1998) can be associated to the input of energy due to the income of hot plasma originating in the close environment of Io (Hess et al., 2008a), whereas short timescale bursts can be associated to the propagation of energetic electrons (Ellis, 1965) along the IFT.

This paper will focus on the informations about the local plasma parameters carried by the latter short (S-) or millisecond bursts (shown in Fig. 1).

The S-bursts are intense, discrete (often quasi-periodic) bursts emitted in the decameter radio range, near the local electron cyclotron frequencies f_{ce} in the vicinity of the planet (i.e. the emission frequency f is proportional to the magnetic field B at the point of emission). Their bursty and quasi-periodic time dependence can result from the

*Corresponding author at: Observatoire de Paris - LUTH/CNRS, 5 Place J. Janssen, 92195 Meudon Cedex, France. Tel.: +33 1 45 07 76 98.
E-mail address: sebastien.hess@obspm.fr (S. Hess).

0032-0633/$ - see front matter © 2007 Elsevier Ltd. All rights reserved.
doi:10.1016/j.pss.2008.10.006

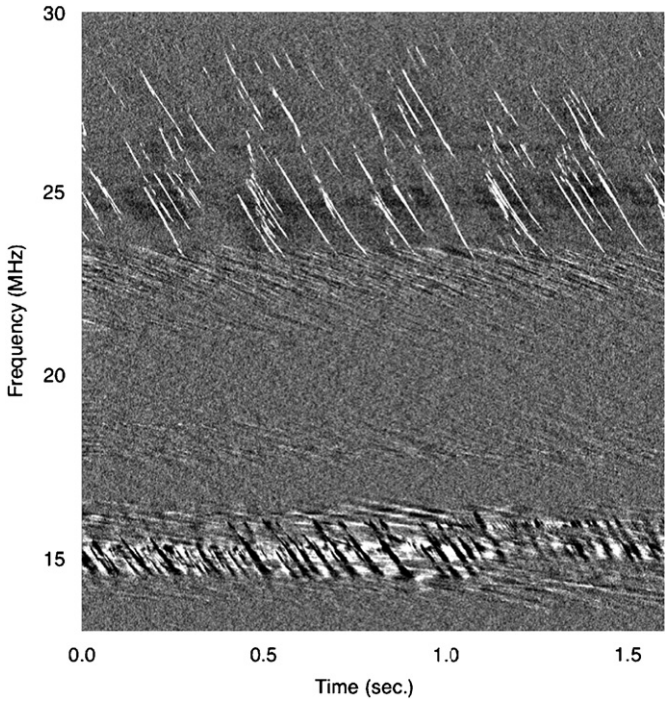

Fig. 1. Dynamic spectrum recorded at the UTR-2 telescope on March 14th, 2005. The time is given from the 5350th second of the day. The S-bursts are the intense drifting structures at frequencies >24 MHz. The nature of the dark (below the background) structures around 14–16 MHz is still unexplained The fainter, more slowly drifting modulations below 24 MHz are not addressed in the present study.

electron acceleration by resonant Alfvén waves (Hess et al., 2007b). One of the main characteristics of these bursts (which will be exploited in this paper) is that they present a negative drift in the time–frequency plane. Since the emission frequency f is proportional to the magnetic field B (which decreases with the distance from Jupiter) the electrons responsible for the emission move away from Jupiter. By measuring the drift rates, we can deduce the electron velocity parallel to the magnetic field lines, the total energy and the pitch angle of the emitting electrons along the IFT, given some assumptions regarding the ! properties of the bursts—adiabatic motion of the emitting electrons out of localized acceleration regions—proposed by Ellis (1965) and verified by Zarka et al. (1996) and Hess et al. (2007a).

Hess et al. (2007a) used these properties to perform a statistical study of the accelerated electron energy (found to be ~4 keV) and to reveal acceleration structures consistent with electric potential drops (with a mean amplitude of ~1 keV). Since their data set was spread over one year, their results are long term averages which do not carry any information about the evolution of the energy and acceleration during a S-burst storm.

In this paper we characterize this evolution of the acceleration structures using high resolution data covering a whole S-burst storm.

In Section 2 the adiabatic model which describes the frequency drift of the millisecond bursts is detailed. In Section 3 we present the data. Section 4 presents some global results about the electron energy determination. The evolution of the electron energy is detailed in Section 5, and the amplitude and motion of the acceleration structures is studied in Section 6. Appendix A describes the method used to derive the electron energy (as a function of altitude) from the data.

2. Adiabatic model

The adiabatic model was proposed as an explanation of the generally negative S-burst drift rates in the time–frequency plane (Ellis, 1965). In this model the emission is due to electrons reflected by magnetic mirror effect (at a local cyclotron frequency called the mirror frequency f_{mirror}) and emitting as they move along the field line at the local cyclotron frequency f_{ce}. The S-burst drift rate $\mathrm{d}f/\mathrm{d}t$ can be measured on the observed dynamic spectra and is connected to the motion of the emitting electrons by

$$\frac{\mathrm{d}f}{\mathrm{d}t} = \frac{\mathrm{d}f_{ce}}{\mathrm{d}s}\frac{\mathrm{d}s}{\mathrm{d}t} = \frac{\mathrm{d}f_{ce}}{\mathrm{d}s} v_{\parallel}(f_{ce}) \tag{1}$$

where $v_{\parallel}$ is the radio source (i.e. the emitting electrons) parallel velocity, chosen to be positive for up-going electrons. The derivative $\mathrm{d}f_{ce}/\mathrm{d}s$ is directly deduced from the Jovian magnetic field model and $v_{\parallel}(f_{ce})$ is deduced from Eq. (1). The adiabatic motion of the emitting electrons without acceleration by parallel electric fields is the baseline model proposed by Ellis (1965). It consists in the conservation of the magnetic moment μ and the kinetic energy K. In order to improve the clarity of the equations, the magnetic moment is defined, in the present paper, as

$$\mu = v_{\perp}^2(f_{ce})/f_{ce} = v^2/f_{mirror} \tag{2}$$

and the electron velocities are given by

$$v_{\perp}^2 = \mu f_{ce} \tag{3}$$

$$v_{\parallel}^2 = v^2 - \mu f_{ce} \tag{4}$$

where v is the electrons velocity. The kinetic energy $K \propto v^2$ and magnetic moment μ of the emitting electrons are the two parameters characterizing the adiabatic motion and they can be deduced from the drift rate measurements by a linear fit:

$$v^2 - \mu f_{ce} = \left(\frac{\mathrm{d}f}{\mathrm{d}t} \Big/ \frac{\mathrm{d}f_{ce}}{\mathrm{d}s}\right)^2 \tag{5}$$

Fig. 2a shows an example of a theoretical drift rate versus frequency as given by the adiabatic model and Fig. 2b shows the corresponding parallel kinetic energy $K_{\parallel}$ ($=\frac{1}{2}mv_{\parallel}^2$ with m the mass of the electron).

As in Hess et al. (2007a), we observe the presence of localized acceleration regions where the parameter $v_{\parallel}^2$ evolves abruptly in a narrow region of the IFT (>10% on ~1000 km). In other words, the parallel energy deduced from measurements presents linear decreases in some frequency ranges separated by acceleration ranges. It is thus possible to fit the linear ranges by line segments

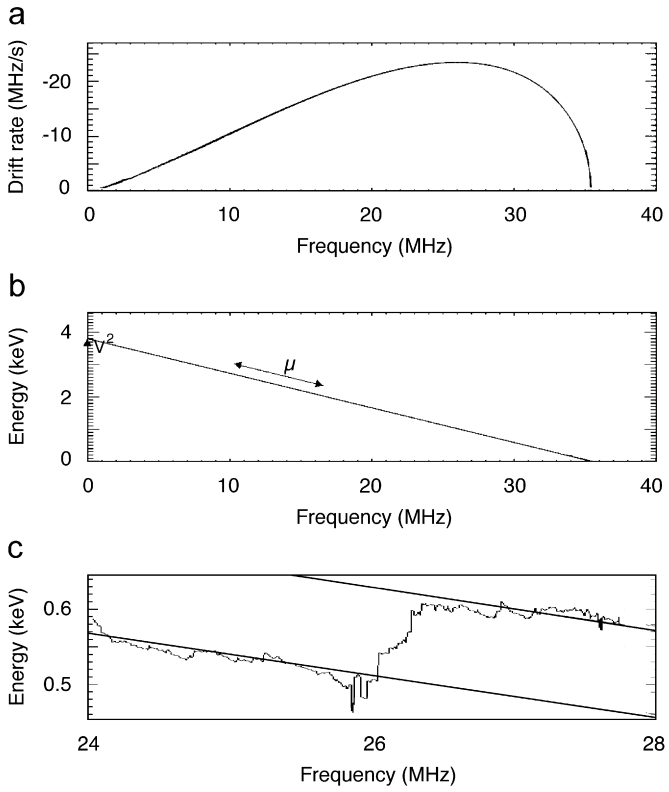

Fig. 2. (a) Drift rate as a function of frequency in the adiabatic model. The continuous line stands for $K = 3.8$ keV and $\mu = 107$ eV/MHz (typical values according to Hess et al., 2007a). (b) Parallel kinetic energy of the emitting electrons $K_{\parallel}(f)$ deduced from the adiabatic model. The parameters are the same as above: the parallel energy at $f = 0$ MHz is the total energy and the slope gives the magnetic moment. (c) Parallel kinetic energy $K_{\parallel}$ measured in our data at the time $t = 5350$ s of the day. It shows two adiabatic segments (24–26 and 26–28 MHz) with the same magnetic moment μ (same slope) separated by a purely parallel acceleration region.

("adiabatic segments"). Fig. 2c shows an example of two adiabatic segments separated by an acceleration region. It corresponds to the parallel kinetic energy $K_{\parallel}$ measured in the UTR-2 data at the time $t = 5350$ s (UT) of Fig. 3.

3. Observations

The observations consist of 230 waveform samples recorded at the Kharkov UTR-2 radiotelescope during the S-burst storm on March 14th 2005. The data and the instrumentation used are described by Ryabov et al. (2007). A windowed Fourier transform and a high pass filtering (in order to remove the long duration emissions which are not in the scope of our study) were performed on these waveforms to obtain 230 dynamic spectra, with a resolution of 0.8 ms in time and 8 kHz in frequency. The duration of each dynamic spectrum is 6.2 s and the recording are done every 15 s (Hess et al., 2007a) showed that the timescale of the energy and the magnetic moment variations is longer than some tens of seconds. Therefore, we measure one average drift rate versus frequency for each dynamic spectrum in order to obtain a quasi-continuous series of drift rates, each representative of a time interval of $\simeq 15$ s. This is sufficient to observe the evolution of the electron characteristics.

In the dynamic spectrum shown in Fig. 1, the bright drifting structures in the range 22–30 MHz are S-bursts.

The origin of the dark drifting structures (with intensity smaller than the background) shown in Fig. 1, is uncertain. They seem to have the same drift as the S-bursts and approximately the same occurrence periodicity (Riihimaa et al., 1981).

The other faint drifting features have a drift rate of ~ 3 MHz/s nearly independent of time and frequency. Their drift rate is different from the S-bursts and are thus out of the scope of this paper.

4. Fit of the adiabatic segments

An automated recognition of the adiabatic segments is performed on the data set. The method is described in Appendix A.

4.1. Magnetic moment and noise

Fig. 3c shows the result of the detection of the adiabatic segments as a diagram of the total kinetic energy K along the segments versus time and frequency. Most of the adiabatic segments corresponds to energy comprised between 2 and 4.5 keV but at some times the energy may be as high as ~ 5 keV or as low as ~ 1 keV.

In the present data all the accelerations were found to be parallel, thus to a given time or longitude corresponds only one value of the magnetic moment μ. Fig. 4a shows the evolution of the magnetic moment with Io's longitude (i.e. with time). This evolution will be discussed in more details in the next section. It appears to be relatively smooth, except for some fluctuations corresponding to the times when Fig. 3c shows large fluctuations of the energy. Assuming that these peaks are only due to the noise in the data, we smooth the evolution of the magnetic moment μ and recompute the energy with these new values of μ (dashed curve in Fig. 4a).

Fig. 3d shows the total kinetic energy versus time and frequency assuming a smoothed evolution of the magnetic moment. It shows a clearer energy evolution versus time and frequency which will be discussed in the next section. Hereafter we will consider only the results with the smoothed magnetic moment evolution.

4.2. Accuracy

Fig. 4b presents the error on the energy determination δ_K of the fit without magnetic moment smoothing versus time:

$$\delta_K(t) = \sigma_K(t)/\langle K\rangle(t) \quad (6)$$

where $\sigma_K(t)$ is the standard deviation of the energy and $\langle K\rangle(t)$ is the averaged total kinetic energy at time t.

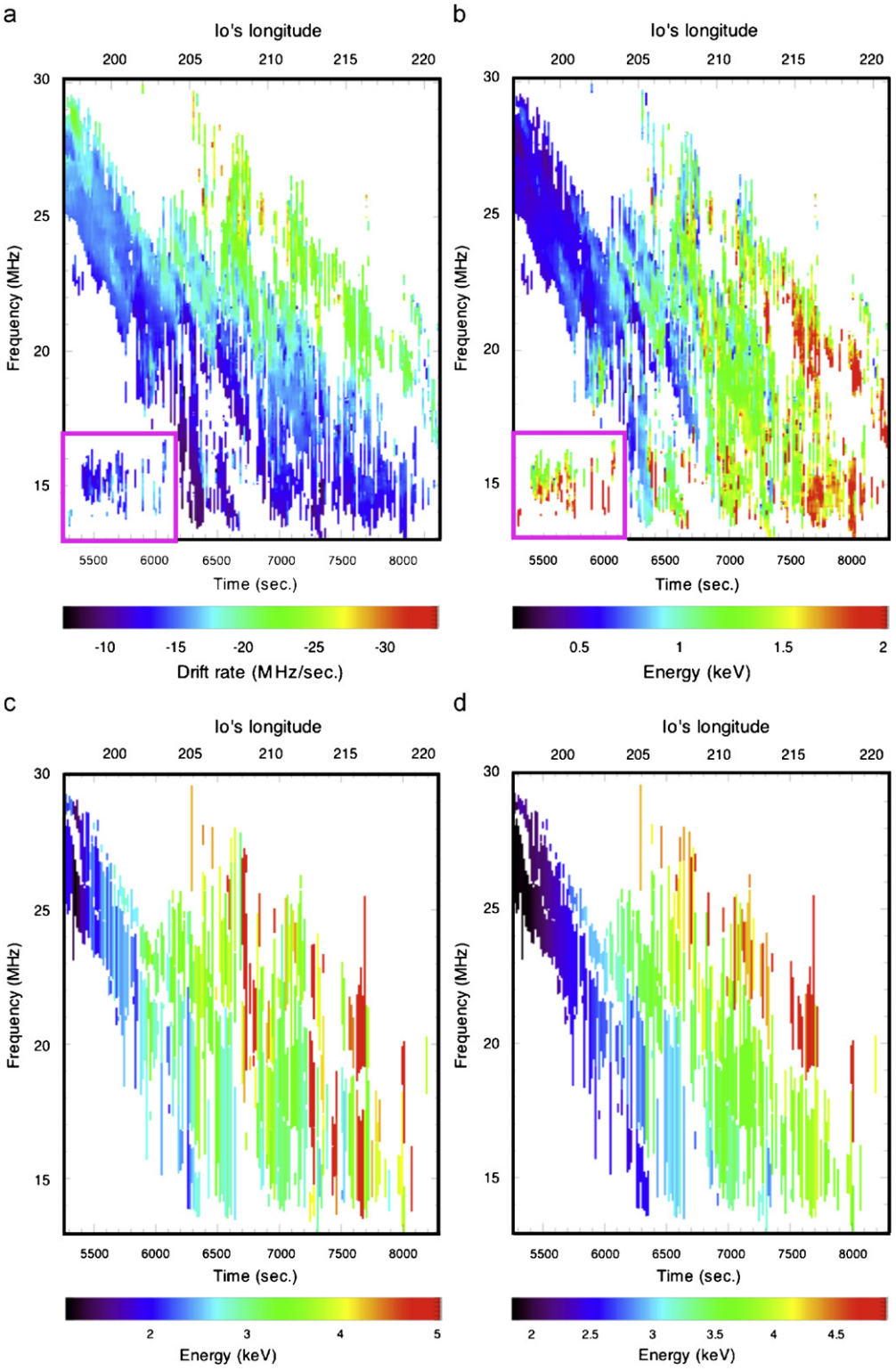

Fig. 3. (a) Drift rate versus frequency (dependent on the altitude) and time (or longitude) measured from the data by a windowed Radon transform. The time is given in seconds, starting from 0.00 UT on 14/03/2005. The measurements surrounded by the pink line corresponds to the dark (intensity below the background) drifting structures shown in Fig. 1. (b) Parallel kinetic energy versus frequency and time derived from the adiabatic model. The parallel kinetic energy decreases with frequency in the adiabatic model, thus any increase of $K_{\parallel}$ corresponds to an acceleration phase. On a timescale of $\sim$1000 s, the energy is seen to increase. (c) Energy of the electron as obtained from the adiabatic segments fitting. A secular ($\tau\sim$1000 s) increase over time of the energy is shown, although abnormally high energies are seen at some times. (d) Energy of the electron as obtained from the adiabatic segments fitting with smoothed magnetic moment μ. The increase of the energy over time and toward high frequency is evidenced.

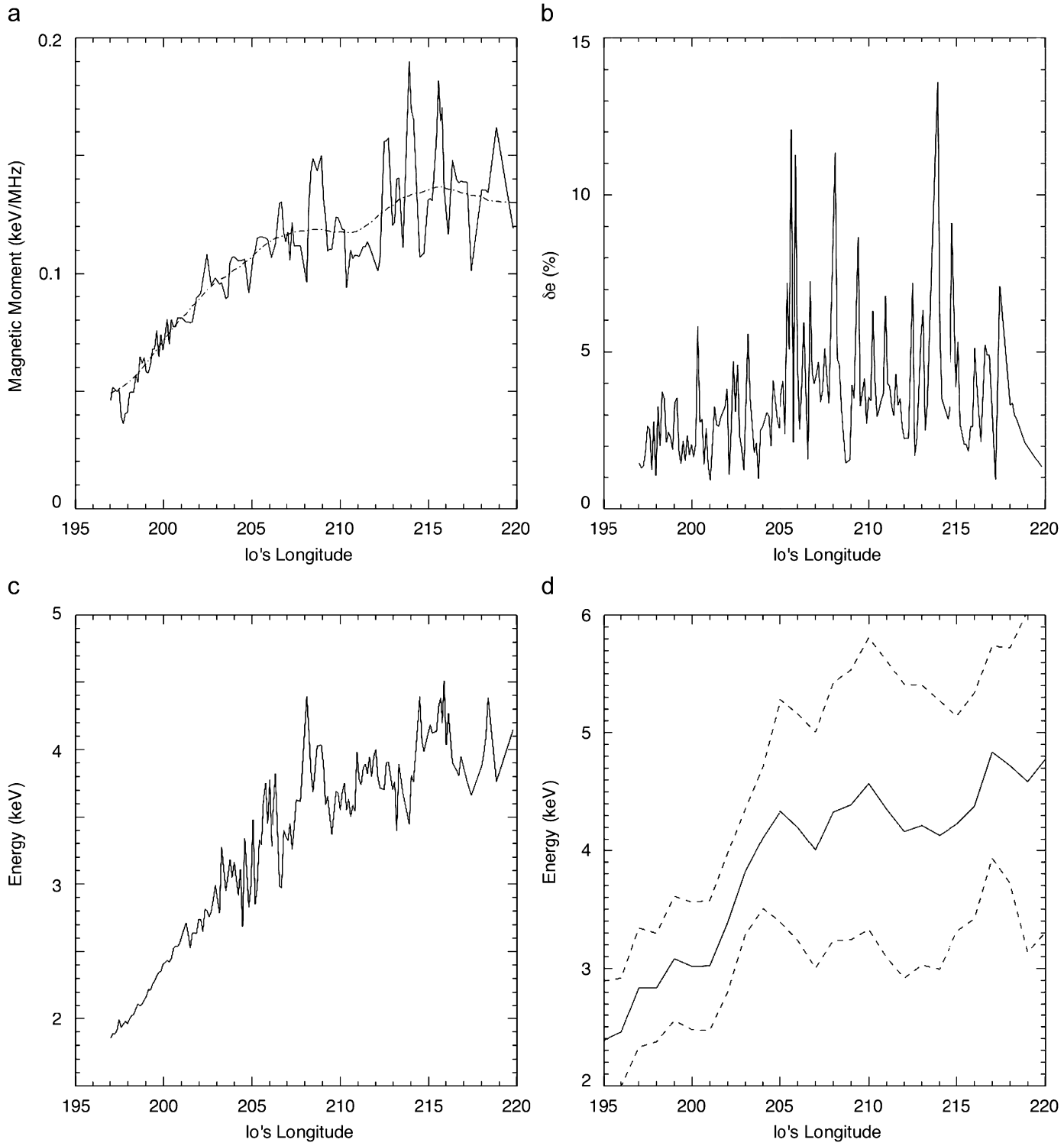

Fig. 4. (a) Magnetic moment of the emitting electrons fitted (full line) and smoothed (dot-dashed line). (b) Error in the fit of the energy in percent (fit without smoothed magnetic moment). (c) Mean energy of the electrons as a function of longitude, obtained from the adiabatic segments fitting with a smoothed magnetic moment. The emitting electron energy increases with increasing longitude. (d) Mean energy as a function of longitude measured from the data presented by Hess et al. (2007a). The dashed lines represent the standard deviation. The latter data were recorded over one year and give a statistical evolution of the energy which is comparable to the evolution seen over one whole S-burst storm.

The mean value of the error is 3.2% both for μ-smoothed and non-smoothed fits. It corresponds to a mean error of 100 eV on the whole longitude range, but only to 50 eV for the first 10° range of longitude. This accuracy permits us to detect weak acceleration regions. The accuracy on the acceleration amplitude vary from a few tens of eV to a few hundreds of eV (the latter concerning the accelerations seen at the border of the emission range).

4.3. Below background drifting structures

The drifting structures appearing with intensity below the background in Fig. 1 have drift rates $\mathrm{d}f'/\mathrm{d}t$ similar to those of the S-bursts (boxed in Fig. 3a). Thus they may also result from electrons in adiabatic motion. Since their drift rate measurements are too noisy, no adiabatic segments can be fitted to their profile of parallel kinetic energy. Nevertheless, if we assume that they are generated by electrons in adiabatic motion (with a magnetic moment μ supposed equal to those of simultaneous S-bursts) they correspond to electron kinetic energies $\langle K' \rangle$:

$$\langle K' \rangle \propto \left(\frac{\mathrm{d}f'}{\mathrm{d}t} \Big/ \frac{\mathrm{d}f_{ce}}{\mathrm{d}s} \right)^2 + \mu f_{ce} \tag{7}$$

The energies obtained this way are within 10% of the S-burst electron energy. Some adiabatic (fitted on the S-burst parallel kinetic energy) segments can even be extended to the frequency range of the dark structures and then fit parts of these structures (basically those appearing in green in the boxed region of Fig. 3b). It suggests strong similarities in the generation of these structures and of the S-bursts. Then dark structures could correspond to resonant cyclotron absorption of background radio emissions by electrons with a distribution different from that generating the S-bursts emission (Gopalswamy, 1986). This remains to be investigated.

5. Longitude dependence of the electron energy

Fig. 3d shows the dynamic spectrum of the total kinetic energy. The mean energy of the electrons is found here to be 3.2 keV which is consistent with the results of Zarka et al. (1996) and Hess et al. (2007a).

For a given time the energy of the emitting electrons increases towards high frequencies. This is due to the fact that all the acceleration regions detected in our data accelerate the electrons toward Jupiter (where $f \sim f_{ce}$ is higher). This property was already seen by Hess et al. (2007a).

Fig. 3d shows that the energy also increases with time. But the time of emission can be translated into the longitude of the emitting flux tube. Fig. 4c shows the evolution of the averaged electron energy versus Io's longitude. We can see a steep and steady increase of the electron energy between Io's longitude 197° and 210°. This evolution could be purely conjunctural, but Fig. 4d, where the statistical evolution of the energy from the data of Hess et al. (2007a) is displayed, shows a comparable evolution of the same order of magnitude. Thus this energy increase must be the consequence of the longitudinal dependence of the acceleration process.

Since all the parameters controlling the emission of decameter radio waves are still not known, we can only propose a possible cause for the increase of energy: the energy flux Φ injected in the IFT can be estimated from the convective electric field E_{conv} generated by the Io's velocity V_{Io} relative to the torus and by the Alfvén conductance Σ_A (Neubauer, 1980; Goertz, 1983):

$$\Phi \propto E_{conv}^2 \Sigma_A \sim V_{Io}^2 B_{Io} \sqrt{\frac{\rho_{Io}}{\mu_0}} \tag{8}$$

where B_{Io} and ρ_{Io} are the magnetic field and plasma density at Io. As Io enters the torus in the considered range of longitude, the density ρ_{Io} increases and thus the flux of energy injected in the IFT Φ increases too. This increase is weak (a few percent) but Eq. (8) is a first order approximation. Alfvén wave reflection, filamentation (Chust et al., 2005), non-linear effects (Jacobsen et al., 2007) may play an important amplifying role. Further analysis is needed for unveiling the connection between the Io-Jupiter interaction intensity and the energy of the electrons emitting the S-bursts.

6. Amplitude and motion of the acceleration structures

We detected 199 acceleration regions in the interval studied. Seventy of them were detected between two adiabatic segments having the characteristics of electric potential drops. The 129 others are accelerations detected on the borders of the emission domain (cf. Appendix A.4). The amplitudes of the latter may be slightly less accurately defined. Nevertheless we performed a statistical study of the distribution of the amplitudes of the acceleration regions (Fig. 5).

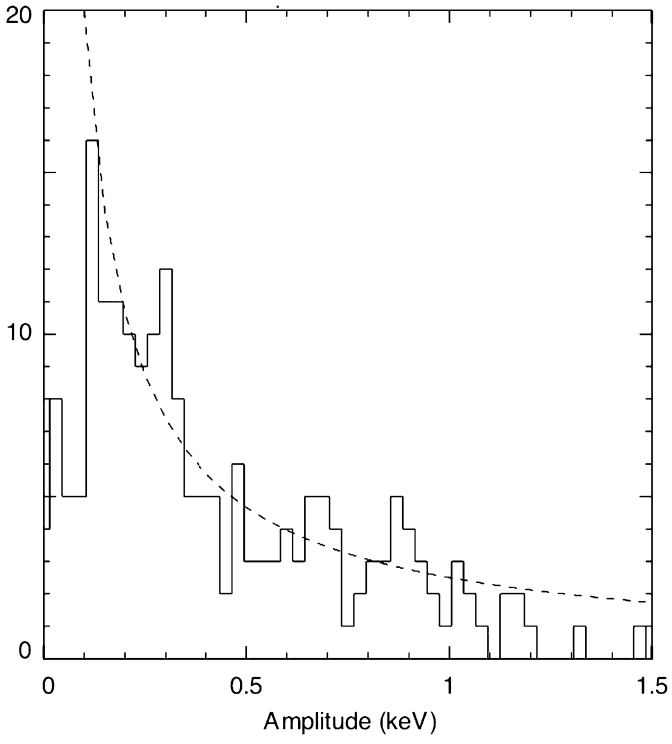

Fig. 5. Distribution of the jumps of energy associated to the acceleration structures. The dashed line is a fit by a scaling law $f(\Delta K) = \Delta K^{-1}$.

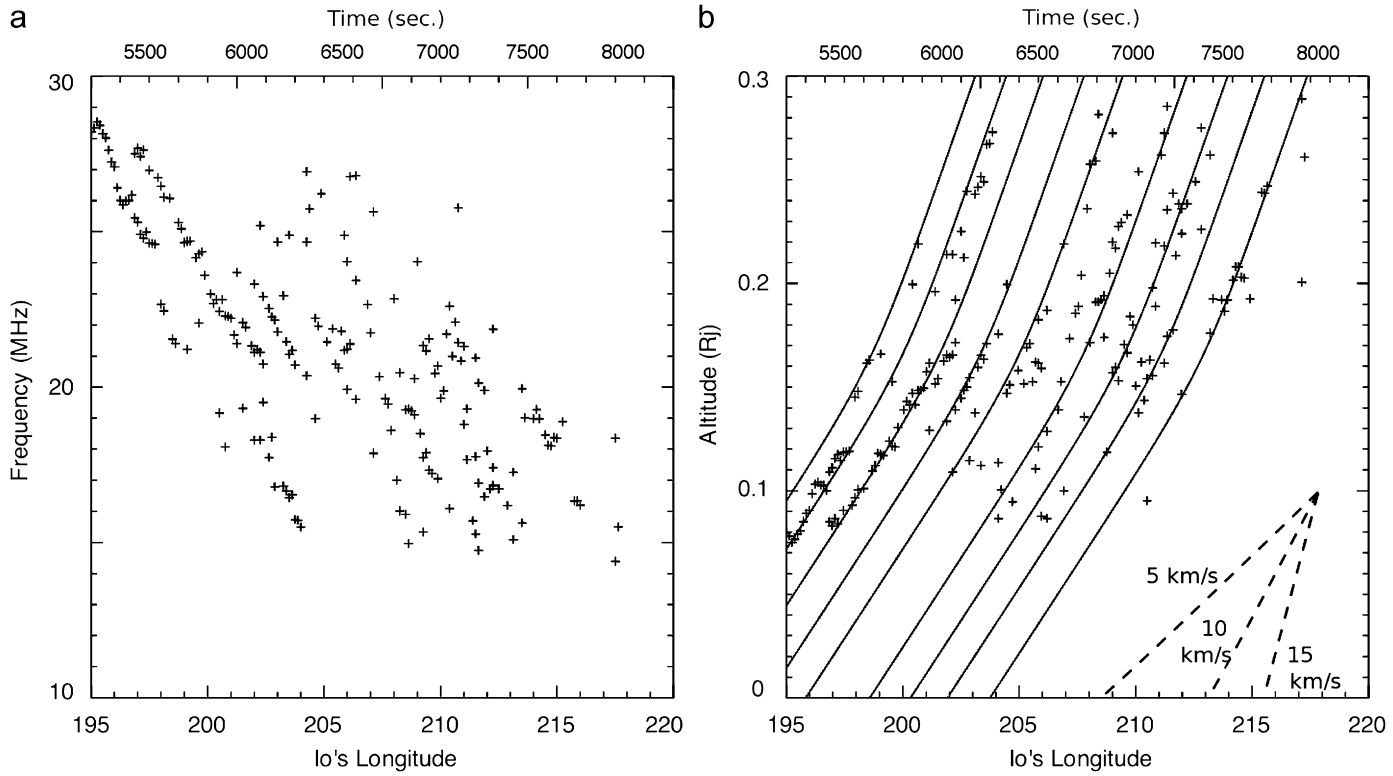

Fig. 6. (a) Position of the acceleration features (potential drops) versus longitude and frequency. The potential drop appears as drifting structures. (b) Position of the potential drops versus time (or longitude) and altitude (above the Jovian ionosphere). The continuous lines show the fits of the drifting structures. The dashed lines show the slope for velocities of 5, 10 and 15 km/s.

We find an overall mean jump of energy $\langle \Delta K \rangle \sim 0.35$ keV, significantly less than the 0.9 keV found by Hess et al. (2007a). This is believed to be due to the better signal to noise ratio of our measurements, which permits us to detect acceleration features with an amplitude down to a few tens of eV (versus a few hundreds of eV for Hess et al., 2007a). The distribution of the jumps of energy $f(\Delta K)$ decreases with increasing amplitude ΔK, with a scaling law ($f(\Delta K) = \Delta K^{-1}$) plotted as a dashed curve in Fig. 5. The low number of acceleration events with an amplitude smaller than 100 eV is due to the limitation of our detection method and to the noise on the data.

Fig. 6a shows the positions of the detected acceleration regions in the time (or Io's longitude)-frequency plane. It shows drifting structures with a negative drift rate, suggesting that the acceleration features move along the IFT away from Jupiter.

In order to measure their velocity we use the VIT4 magnetic model to compute their positions in the time-altitude plane (Fig. 6b). The velocity of the acceleration structures is about 7 km/s below an altitude of 0.2 Jovian radius and 15 km/s above, which is much slower than the Alfvén velocity ($\sim c$) or the emitting electron velocity ($\sim 0.1c$), but of the same order of magnitude as the plasma sound velocity c_s:

$$c_s = \sqrt{\frac{T_e + 3T_i}{m_i}} \tag{9}$$

The measured acceleration structure velocity corresponds to the sound velocity of a plasma with an ion and electron temperature of 0.14 eV below 0.2 Jovian radius and an electron temperature of 1.5 eV above, which is consistent with the estimation of the plasma temperature in the Jovian auroral region (Grodent and Gérard, 2001; Bougher et al., 2005). The fit of the acceleration structure motion by the sound speed (with two populations of electrons) is shown by the lines in Fig. 6b. It has been performed by assuming a hydrostatic law for the cold (0.14 eV) component and a constant density of the hot (1.5 eV) component which is 10^4 times lower than the cold one at the ionosphere boundary.

We also see that the acceleration structures can subsist up to 10 min and seems to occur with a quasi-period of about 200 s. It should be noted that the acceleration structures are not directly related to the observed emission bands shown by Fig. 3a (the drift in frequency and the localization in time and frequency are different). However, Arkhypov and Rucker (2008) proposed that the variation of the direction of emission due to the electron acceleration may cause such observed emission bands.

7. Discussion and conclusion

The observation of the Io-controlled millisecond bursts permits us to probe the energetic electrons in the IFT, close to the Jovian auroral region.

We found a dependence of the electron energy relative to the longitude, that may be connected to the non-axisymmetric structure of the Jovian magnetic field and to the inclination of the Io plasma torus on the jovicentric equator. The energy of the electrons is correlated with the energy flux derived by Neubauer (1980) and Goertz (1983) in their model of IFT unipolar inductor.

We also found evidence of acceleration structures, at all time (or longitude). These structures accelerate the electrons towards Jupiter in a direction parallel to the magnetic field (the electron magnetic moment is unchanged). They correspond to electric potential drops of a few hundreds of volts. Such structures were already detected (Hess et al., 2007a) in data recorded at the Nançay decametric radio-telescope. But in this previous study, the available data were segmented, and did not allow for the study of their duration and velocity. The data obtained in Kharkov and analyzed in the present paper allow us to conclude that the acceleration structures can subsist for about 10 min and that they move along the magnetic field with an upward velocity (relatively to Jupiter) that is of the same order of magnitude as the ion sound velocity.

Their long duration implies that they are quasi-stationary structures. As the acceleration structures are seen purely parallel, localized and having an amplitude much larger than the plasma temperature, their behavior is consistent with those of strong double layers (electric potential drops) observed in Earth's magnetosphere (Block, 1978, 1988).

Many models describe the strong potential drops with a velocity about the ion sound velocity. They invoke ion acoustic waves (Cattell et al., 1998; Singh et al., 2005), ion holes (Singh et al., 2005), solitons (Das et al., 1998) or electrostatic shocks (Pottelette et al., 2003) as potential drop generation mechanisms. They have been seen in the terrestrial auroral region (Gorney et al., 1985; Bruning et al., 1990; Mäkelä et al., 1998) and have been modeled (Ergun 2002a, b; Main et al., 2006), showing a drift at the sound speed of the plasma.

We can expect more analogies between the acceleration structures inferred from the present analysis and the strong double layer observed in the Earth auroral zone. Of course, the processes of injection of energy is different: in the case of Earth, it is related to the interaction of the auroral zone with substorm phenomenon in the magnetospheric tail, while in the case of the IFT, it is related to the motion of Io in the plasma torus. But, for both cases, the acceleration structures are observed close to the planet (1000–10 000 km in the case of the Earth, and about 6000–20 000 km for Jupiter), and far from the region where the energy is injected. The connection between the acceleration region and the region of injection of energy is made through a forced current (that can be stationary or associated to Alfvén waves).

We notice that in the case of Earth, the cyclotron maser instability triggers radio emissions that are below the ionospheric cut-off, and the waves (the auroral kilometric radiation, or AKR) can only be observed onboard spacecraft. These radiations were discovered in the space era, and are investigated through in situ measurement, as are the strong double layers.

In the case of Jupiter, the radio emissions resulting from the cyclotron maser instability can be (partly) observed from the ground ($f > 10$ MHz, the Earth's ionospheric cutoff), and be used as a tool for remote sensing of other structures, such as the acceleration structures presented in this paper, that have not yet been measured in situ at Jupiter.

Are there such acceleration structures present at higher altitudes above Jupiter? We cannot answer this question with the use of data measured on Earth, because beyond 25 000 km, the local gyrofrequency is of the order of 5 MHz, and waves at such a frequency are below the Earth ionospheric cut-off. The only chance to make such an analysis is to use data measured onboard a satellite. But nowadays, the sampling rate of the data from spacecraft do not allow to resolve the millisecond bursts. With probes exploring the Jovian auroral zones, such as JUNO, the region of emission of the decametric radiation will be explored, and in situ measurement will be able to confirm, or not, the existence of the acceleration structures discussed in the present paper.

Appendix A. Method

In order to process systematically the whole data described in Section 3, we have implemented a pipeline that starts from the dynamic spectra, such as shown in Fig. 1, and produces fitted adiabatic segments of constant energy, such as shown in Fig. 2c. For that purpose we:

(1) measure the drift rate of the S-bursts $\mathrm{d}f/\mathrm{d}t$ (this is made in Appendix A.1 and Fig. 3a);
(2) using a magnetic field model, get the energy $K_{\parallel}$ of the electrons parallel to the magnetic field lines (Appendix A.2 and Fig. 3b);
(3) applying an adiabatic model to obtain the electron kinetic energy K by fitting their parallel kinetic energy versus frequency $K_{\parallel}(f)$ with linear segments, possibly separated by acceleration events.

A.1. Measurement of the frequency drifts

Each drift rate is computed by applying a windowed Radon transform on the corresponding dynamic spectrum. The Radon transform is obtained by an integration of the 2D Fourier transform of the dynamic spectrum along a straight line centered at the origin of the Fourier domain. The value of the intensity at the coordinates (k_f, k_t) of the Fourier domain corresponds to the intensity of periodic features having a slope in the time–frequency domain given by $\theta = \arctan k_f/k_t$. The integration along a straight line in the Fourier domain, centered at its origin, is an integration of the intensities of all the Fourier modes corresponding to

a given slope in the time–frequency domain. Thus the Radon transform of a dynamic spectrum gives us the integrated intensity of the linear features $I(\theta)$ versus their slope θ (Dumez-Viou et al., 2005). We compute it on a window sliding along the frequency dimension in order to measure the drift rate of the features as a function of frequency. The intensity of the Radon transform has a maximum for an angle corresponding to the slope of the dominant drifting features of the dynamic spectrum and has a minimum for angles perpendicular to this. Thus we introduce the "contrast" versus angle $C(\theta)$ by

$$C(\theta) = I(\theta)/I(\theta + 90^\circ) - 1 \quad \text{(A.1)}$$

The maximum of the function corresponds to the slope of the drifting structures. If there is no drifting features we obtain $C(\theta) = 0$ for every angle θ. We have set a threshold for the maximal value of $C(\theta)$ above which we consider that a drifting structure is present and its slope measured. The noise on the data introduces a noise on the contrast which is measured to be ~0.2, thus we set the threshold value to 0.3.

The weak drifting structures, having a constant drift rate of about 3 MHz/s, appearing in the dynamic spectra (Fig. 1) are not related to the S-bursts, which have drift rates typically exceeding 10 MHz/s. We eliminate the measurements for which the measured drift rate is less than 6 MHz/s. The dark drifting structures appearing at low frequency in Fig. 1 have drift rates similar to the S-bursts and cannot be eliminated. Fig. 3a shows the results of the drift rate measurements on our data set. The part inside the box corresponds to the dark drifting structures appearing in Fig. 1.

The detected S-bursts appear as bands in the time–frequency plane, it may be due to visibility effects. Since the emission is strongly anisotropic, the observer must be in the direction of the emission to see the radio bursts. This direction varies with the energy of the emitting electrons and with frequency (Hess et al., 2008a; Arkhypov and Rucker, 2008).

A.2. Measurement of the parallel kinetic energy

The parallel kinetic energy $K_\parallel$ is obtained from the drift rate through Eqs. (4) and (5). The VIT4 magnetic field model (Connerney, personal communication) is used to compute the gradient of the electron cyclotron frequency along the magnetic field lines ($\partial f_{ce}/\partial s$). The VIT4 model is obtained from the fit in latitude of the galilean satellite footprints and normalized by the Voyager measurements. It is presently the most accurate description of the magnetic field lines connecting Io to Jupiter.

In order to compute the gradient of the magnetic field along the emitting field line, it is necessary to estimate the longitude difference between the "active" radio emitting field line and Io's field line. There is no estimation of the lead angle for the field line emitting S-bursts. For the Io-controlled Jovian arcs, which are closely associated with the S-bursts, Queinnec and Zarka (1998) found a mean lead angle about 20°. Lower angles (between 8° and 20°) are found by Hess et al. (2008b) who reproduce the arc shape from basic assumptions. Large range of angles (between 5° and 57°) are found by Arkhypov and Rucker (2007) from a more indirect method. In UV the lead/lag angle has been determined to be around 0° by the longitude range considered here (Clarke et al., 1998; Prangé et al., 1998).

As this angle has a weak influence on our results we take here a null lead/lag angle. Fig. 3b shows the parallel kinetic energy determined from the drift rate measurements. The boxed region is further discussed in Section 4.

A.3. Detection of the adiabatic segments

The parameters defining the adiabatic motion of the emitting electrons (energy K and magnetic moment μ) are not necessarily uniform over the whole range of observed altitudes, thus the linear relation between the parallel kinetic energy and the frequency can be matched in several frequency intervals separated by narrow acceleration intervals. In order to measure the energy and the magnetic moment of the emitting electrons we have to fit the adiabatic ranges by line segments, as in Hess et al. (2007a).

For all frequency intervals (i.e. for all couples of minimum and maximum frequencies $(f_{\min}, f_{\max})$ with $f_{\max} - f_{\min} > 1.5$ MHz), we fit a segment by

$$v^2_{seg,\parallel} = Median(v^2_{mes,\parallel} + \mu f_{ce}) - \mu f_{ce} \quad \text{(A.2)}$$

where $v_{mes,\parallel}$ is the measured parallel velocity (directly deduced from the drift rate) and $v_{seg,\parallel}$ the fitted value (by the fit of the adiabatic segment). We choose the median rather than the mean value because it is less sensitive to extreme values. The only independent variable of the fit is then (μ). The segment (i.e. the value of μ) is fitted by minimization of a coefficient Ξ

$$\Xi = \frac{\sigma_K}{\langle K_\parallel \rangle c_{cor}} \quad \text{(A.3)}$$

where σ_K is the standard deviation (in term of kinetic energy) between the measurements and the fit, $\langle K_\parallel \rangle$ the mean parallel energy on the whole bandwidth (13–30 MHz) and c_{cor} the correlation coefficient between the measurements and the segment. This method permits to get, for each possible frequency range, the segment which minimizes the standard deviation with the data and maximizes the correlation with it. The segments for which $\Xi > 0.2$ or/and $c_{cor} < 0.7$ are eliminated because they are not considered as good fits of the data.

A combination of the segments obtained in this way is used to fit the whole bandwidth measurements. The selected segments are chosen without overlap and minimizing Ξ/N, with N being the "length" of the frequency interval associated with the segment. (This permits to remove a bias which favors the short segments which are easier fitted.)

A.4. Detection of the parallel acceleration structures

The presence of several consecutive adiabatic segments in the same profile of the parallel kinetic energy (corresponding to a given 6.2 s long dynamic spectrum) shows the presence of acceleration ranges (Hess et al., 2007a). If the variation of the magnetic moment between two consecutive segments $\Delta\mu/\mu$ does not exceed 50%, the acceleration is considered to be mostly parallel. In our data, all the acceleration events deduced from the presence of several adiabatic segments match this criterion (it was not the case in Hess et al., 2007a). Thus we consider that the accelerations between the successive adiabatic segments are mainly in the parallel direction, and that the magnetic moments of the electrons are equal in the two segments.

Therefore, we fit (again by minimizing Ξ) both adiabatic segments and the acceleration region in between by a shape composed of two parallel segments (corresponding to the adiabatic segments) connected by a third straight line (the acceleration event). The fit must again satisfy the same conditions as for the individual segments ($\Xi<0.2$ and $c_{cor}>0.7$).

The method of detection of the adiabatic segments requires that the adiabatic segments have an extent in frequency larger than 1.5 MHz. If an acceleration occurs near the highest or lowest emission frequency, the adiabatic segment located above (in frequency) or below it may be missed. To detect these accelerations we try systematically to fit an energy drop on the borders of the emissions region. We do it the same way as for the drop between two detected segments. We consider that an energy drop is present if the fitted shape matches again the conditions $\Xi<0.2$ and $c_{cor}>0.7$ and if the segments added in this way cover a frequency range at least of 0.5 MHz.

References

Arkhypov, O.V., Rucker, H.O., 2007. Amalthea's modulation of Jovian decametric radio emission. Astron. Astrophys. 467, 353–358.

Arkhypov, O.V., Rucker, H.O., 2008. S-bands of Jovian decametric emission. Astron. Astrophys. 482, 1009–1014.

Bagenal, F., 1994. Empirical model of the Io plasma torus: Voyager measurements. J. Geophys. Res. 99, 11043–11062.

Block, L.P., 1978. A double layer review. Astrophys. Space Sci. 55, 59–83.

Block, L.P., 1988. Acceleration of auroral particles by magnetic-field aligned electric fields. Astrophys. Space Sci. 144, 135–147.

Bougher, S.W., Waite, J.H., Majeed, T., Gladstone, G.R., 2005. Jupiter thermospheric general circulation model (JTGCM): global structure and dynamics driven by auroral and Joule heating. J. Geophys. Res. (Planets) 110 (E9), 4008–+.

Bruning, K., Block, L.P., Marklund, G.T., Eliasson, L., Pottelette, R., 1990. Viking observations above a postnoon aurora. J. Geophys. Res. 95 (14), 6039–6049.

Cattell, C., Wygant, J., Dombeck, J., Mozer, F.S., Temerin, M., Russell, C.T., 1998. Observations of large amplitude parallel electric field wave packets at the plasma sheet boundary. Geophys. Res. Lett. 25, 857–860.

Chust, T., Roux, A., Kurth, W.S., Gurnett, D.A., Kivelson, M.G., Khurana, K.K., 2005. Are Io's Alfvén wings filamented? Galileo observations. Planet. Space Sci. 53, 395–412.

Clarke, J.T., Ben Jaffel, L., Gérard, J.-C., 1998. Hubble Space Telescope imaging of Jupiter's UV aurora during the Galileo orbiter mission. J. Geophys. Res. 103, 20217–20236.

Das, G.C., Tagare, S.G., Sarma, J., 1998. Quasipotential analysis for ion-acoustic solitary waves and double layers in plasmas. Planet. Space Sci. 46, 417–424.

Delamere, P.A., Bagenal, F., Ergun, R., Su, Y.-J., 2003. Momentum transfer between the Io plasma wake and Jupiter's ionosphere. J. Geophys. Res. (Space Phys.) 108 (A6), 11-1.

Dumez-Viou, C., Ravier, P., Zarka, P., 2005. Real time detection of natural brief events in a corrupted environment. In: Proceedings of the XXVIIIth General Assembly of the International Union of Radio Science.

Ellis, G.R.A., 1965. The decametric radio emission of Jupiter. Radio Sci. 69D, 1513–1530.

Ergun, R.E., Andersson, L., Main, D.S., Su, Y.-J., Carlson, C.W., McFadden, J.P., Mozer, F.S., 2002a. Parallel electric fields in the upward current region of the aurora: indirect and direct observations. Phys. Plasmas 9, 3685–3694.

Ergun, R.E., Andersson, L., Main, D., Su, Y.-J., Newman, D.L., Goldman, M.V., Carlson, C.W., McFadden, J.P., Mozer, F.S., 2002b. Parallel electric fields in the upward current region of the aurora: numerical solutions. Phys. Plasmas 9, 3695–3704.

Goertz, C.K., 1983. The Io-control of Jupiter's decametric radiation—the Alfven wave model. Adv. Space Res. 3, 59–70.

Goldreich, P., Lynden-Bell, D., 1969. Io, a Jovian unipolar inductor. Astrophys. J. 156, 59–78.

Gopalswamy, N., 1986. A theory of Jovian shadow bursts. Earth Moon Planets 35, 93–115.

Gorney, D.J., Chiu, Y.T., Croley, D.R., 1985. Trapping of ion conics by downward parallel electric fields. J. Geophys. Res. (Space Phys.) 90 (9), 4205–4210.

Grodent, D., Gérard, J.-C., 2001. A self-consistent model of the Jovian auroral thermal structure. J. Geophys. Res. 106, 12933–12952.

Hess, S., Zarka, P., Mottez, F., 2007a. Io-Jupiter interaction, millisecond bursts and field-aligned potentials. Planet. Space Sci. 55, 89–99.

Hess, S., Mottez, F., Zarka, P., 2007b. Jovian S-bursts generation by Alfvén waves. J. Geophys. Res. 112, A11212.

Hess, S., Mottez, F., Zarka, P., 2008a. Generation of the Jovian radio decametric arcs from the Io flux tube. J. Geophys. Res. 113, A03209.

Hess, S., Cecconi, B., Zarka, P., 2008b. Modeling of Io-Jupiter decameter arcs, emission beaming and energy source. Geophys. Res. Lett. 35, 13107–+.

Jacobsen, S., Neubauer, F.M., Saur, J., Schilling, N., 2007. Io's nonlinear MHD-wave field in the heterogeneous Jovian magnetosphere. Geophys. Res. Lett. 34, 10202–+.

Main, D.S., Newman, D.L., Ergun, R.E., 2006. Double layers and ion phase-space holes in the auroral upward-current region. Phys. Rev. Lett. 97 (18), 185001–+.

Mäkelä, J.S., Mälkki, A., Koskinen, H., Boehm, M., Holback, B., Eliasson, L., 1998. Observations of mesoscale auroral plasma cavity crossings with the Freja satellite. J. Geophys. Res. (Space Phys.) 103 (12), 9391–9404.

Moncuquet, M., Bagenal, F., Meyer-Vernet, N., 2002. Latitudinal structure of outer Io plasma torus. J. Geophys. Res. (Space Phys.) 107 (A9), 24-1.

Neubauer, F.M., 1980. Nonlinear standing Alfven wave current system at Io—theory. J. Geophys. Res. 85 (14), 1171–1178.

Pottelette, R., Treumann, R.A., Berthomier, M., Jasperse, J., 2003. Electrostatic shock properties inferred from AKR fine structure. Nonlinear Process. Geophys. 10, 87–92.

Prangé, R., Rego, D., Pallier, L., Connerney, J., Zarka, P., Queinnec, J., 1998. Detailed study of FUV Jovian auroral features with the post-COSTAR HST faint object camera. J. Geophys. Res. 103, 20195–20216.

Queinnec, J., Zarka, P., 1998. Io-controlled decameter arcs and Io-Jupiter interaction. J. Geophys. Res. 103 (12), 26649–26666.

Riihimaa, J.J., Carr, T.D., Flagg, R.S., Greenman, W.B., Gombola, P.P., Lebo, G.R., Levy, J.A., 1981. Fast-drift shadow events in Jupiter's decametric radio spectra. Icarus 48, 298–307.

Ryabov, V.B., Ryabov, B.P., Vavriv, D.M., Zarka, P., Kozhin, R., Vinogradov, V.V., Shevchenko, V.A., 2007. Jupiter S-bursts: narrow-band origin of microsecond subpulses. J. Geophys. Res. (Space Phys.) 112 (A11), 9206–+.

Saur, J., 2004. A model of Io's local electric field for a combined Alfvénic and unipolar inductor far-field coupling. J. Geophys. Res. (Space Phys.) 109 (A18), 1210–+.

Saur, J., Neubauer, F.M., Connerney, J.E.P., Zarka, P., Kivelson, M.G., 2004. Plasma interaction of Io with its plasma torus. Jupiter. The Planet, Satellites and Magnetosphere, pp. 537–560.

Singh, N., Deverapalli, C., Khazanov, I., Puthumbakum, N., Rajagiri, A., 2005. Parallel electric fields in a diverging flux tube with upward current: nature of quasi-static fields. J. Geophys. Res. (Space Phys.) 110 (A9), 5205–+.

Su, Y.-J., Jones, S.T., Ergun, R.E., Bagenal, F., Parker, S.E., Delamere, P.A., Lysak, R.L., 2006. Io-Jupiter interaction: Alfvén wave propagation and ionospheric Alfvén resonator. J. Geophys. Res. (Space Phys.) 111 (A10), 6211–+.

Wu, C.S., 1985. Kinetic cyclotron and synchrotron maser instabilities—radio emission processes by direct amplification of radiation. Space Sci. Rev. 41, 215–298.

Wu, C.S., Lee, L.C., 1979. A theory of the terrestrial kilometric radiation. Astrophys. J. 230, 621–626.

Zarka, P., Farges, T., Ryabov, B.P., Abada-Simon, M., Denis, L., 1996. A scenario for Jovian S-bursts. Geophys. Res. Lett. 23, 125–128.